JOURNAL OF THERMOPHYSICS AND HEAT TRANSFER
Vol. 6, No. 4, Oct.–Dec. 1992

Investigation of Mixed Convection About a Rotating Sphere by Holographic Interferometry

Sheng Mao Tieng* and An Cherng Yan†
National Cheng Kung University, Tainan, Taiwan 70101, Republic of China

The mixed convection flow around a heated rotating sphere is investigated experimentally over a test range of Reynolds numbers from 0 to 33,320, Grashof numbers from 3.07 × 10^5 to 3.21 × 10^5 and inclination angles of rotational axis from 0 deg to 90 deg, by means of a three-dimensional holographic visualization method. A detailed visual analysis of the holographic fringe patterns reveals such interesting flow phenomena as flow separation and reattachment, turbulent zones, and jet eruptions. These are discussed in terms of the interactions between the buoyancy and centrifugal forces. Quantitative results for the thickness of the thermal boundary layer, location of the separation point, and the critical rotational Reynolds number for separation are presented and compared with previous theoretical predictions.

Nomenclature

C_p = specific heat of fluid at constant pressure
D = sphere diameter
g = gravitational acceleration
h = heat transfer coefficient
L_s = characteristic length of a sphere
T_w = sphere wall temperature
T_∞ = ambient temperature
α = rotational angle
β = thermal coefficient of volume expansion
θ = polar angle
κ = thermal conductivity
μ = fluid dynamic viscosity
ν = fluid kinematic viscosity, μ/ρ
ρ = density
ϕ = azimuthal angle
Ω = angular velocity of the sphere

I. Introduction

MIXED convection around a heated rotating sphere and its heat transfer characteristics are of fundamental interest to the fields of geophysics, meteorology, astrophysics, aeronautics, and fluid dynamics. Sir George Stokes,[1] in 1845, was the first to investigate the flow induced by an unheated rotating sphere. Since then many authors[2–7] have concentrated on this problem.

In contrast, a heated sphere rotating in air introduces more complex problems of convection (Singh),[8] such as heat transfer characteristics which were experimentally investigated by Nordlie and Kreith.[9] Kreith and coworkers,[10] in a later paper, experimentally measured this heat transfer process with a thermocouple and studied the velocity boundary layer of a rotating sphere employing a hot wire and smoke visualization method. Although the problems associated with mixed convection have received much attention recently, these studies[11–16] have focused on theoretical and numerical analyses rather than experimental work. Furthermore, since interactions between buoyancy and centrifugal forces complicate the flow, it is considerably difficult to perform a thorough investigation by using theoretical analyses. In view of this point, the flow visualization approach provides a practical and easy technique to study this subject.

In this work, an advanced laser technique, laser holographic interferometry,[17] was employed in order to visualize the mixed convection flow of a heated spinning sphere. The experiment was carried out over Reynolds numbers from 0 to 33,320 and Grashof numbers from (3.07 ~ 3.21) × 10^5. In contrast to previous studies where the vertical rotation axis of the heated sphere was parallel to the direction of gravity, this investigation varied the angle of inclination with respect to the vertical axis, thereby giving a three-dimensional holographic observation of the asymmetric convection induced by an inclined rotation sphere.

II. Experiment

A chrome steel sphere of diameter 35 mm was used in the experiment. It was attached to a rotating shaft driven by a variable-speed DC-motor capable of maintaining rotational rates of up to 7200 rpm. This shaft was designed to be as small as possible in order to minimize heat conduction along it. The surface temperature of the sphere was measured by a microthermocouple probe which was inserted in opposition to the shaft, into a hole (diameter of 1 mm) to a depth of 20 mm. The hole was filled up with insulation (asbestos) to guarantee accurate measurement. A schematic diagram of the test apparatus is shown in Fig. 1.

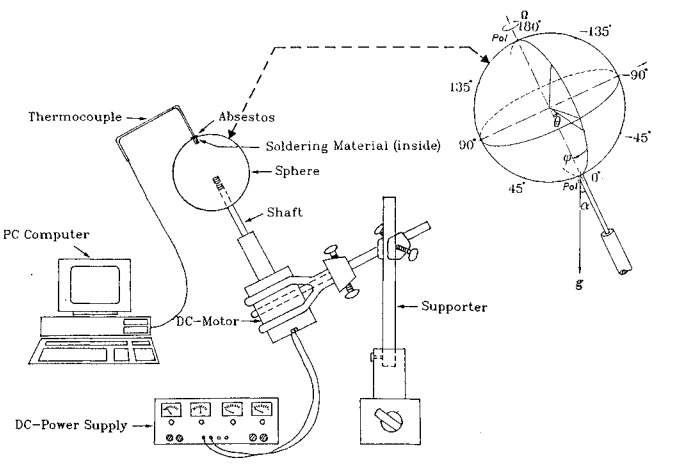

Fig. 1 Schematic diagram of test apparatus.

Received Feb. 25, 1991; revision received July 20, 1991; accepted for publication Aug. 22, 1991.

*Associate Professor, Institute of Aeronautics and Astronautics. Member AIAA.

†Graduate Student, Institute of Aeronautics and Astronautics; currently at Aeronautical Research Laboratory. Chung-Shan Institute of Science and Technology, Taichung, Taiwan, Republic of China.

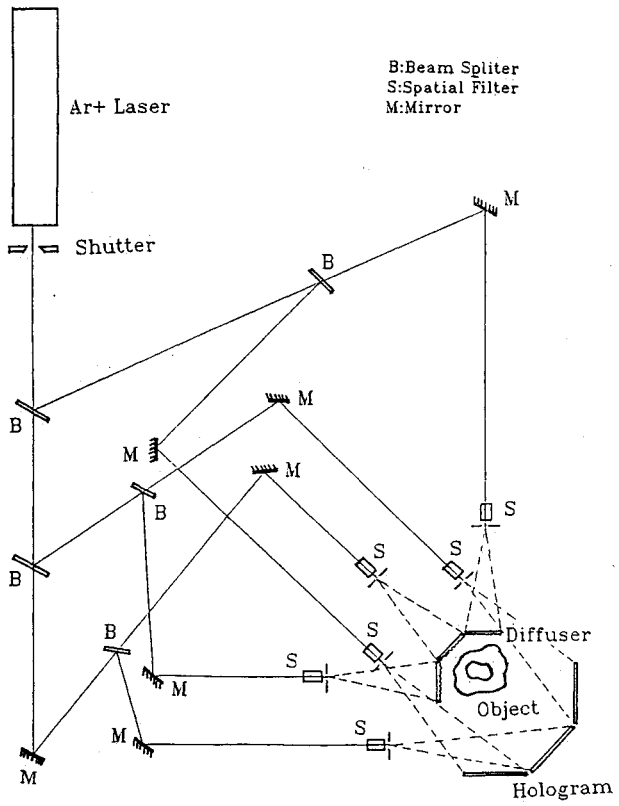

Fig. 2 Schematic diagram of optical test system: laser diffuse-illumination holographic interferometry.

The Biot number of the sphere can be calculated in the following manner, with $L_s = D/6$

$$B_i = \frac{hL_s}{K_s} = \frac{(50)\,[(3.5 \times 10^{-2})/6]}{46} = 0.0063 << 0.1$$

The result indicates that the sphere can be taken as being an isothermal or lumped system at any instant.

A schematic diagram of the optical system designed for diffuse-illumination holographic interferometry is shown in Fig. 2. With this system it is possible to record, from many different directions, the optical pathlengths of light rays as they pass through the flow field. A single frequency Ar^+ laser with wavelength 5145 Å, and output 1.2 W (Innover 306, Coherent Inc. with Etalon) was used as a light source. Three holographic plates (Agfa 10E56 4 × 5 in.) were arranged at a mutual intersection angle of 60 deg for simultaneous recording. Each plate provided a viewing range of about 20 deg.

For further details of the diffuse-illumination holographic interferometry technique, the reader is referred to Refs. 17 and 18. The rotational Reynolds, Grashof, and Prandtl numbers of the sphere[10,11] are defined respectively as

$$Re = \rho\Omega D^2/\mu \tag{1}$$

$$Gr = \beta g(T_w - T_\infty)D^3/\nu^2 \tag{2}$$

$$Pr = \mu C_p/k \tag{3}$$

The experiment covered the range of Re (0–33,320) and $Gr((3.07 \sim 3.21) \times 10^5)$, while Pr was fixed at a value of 0.72.

For each test case, the rotational axis of the heated sphere was inclined at a different angle (0–90 deg) with respect to the direction of gravitational force. The sphere was at first heated by a flame and then rotated at the required speed. When the desired test temperature (about 260–300 deg) was reached, the holograms were photographed using an exposure time of 1/500 s. The holograms were formed from two exposures; one of the stationary sphere at ambient temperature (25°C) and the other of the spinning sphere at the desired temperature and rotational rate. The fringe patterns generated can be directly observed by the unaided eye to change as the viewing angle (direction) is shifted.

III. Results and Discussion

The fringe patterns reconstructed from the hologram provide both reliable qualitative indications of the flow structure, as well as quantitative information about temperature distribution.

A. Flow Visualization

Using different rotational rates, three sets of interferograms at rotational angles α = 0, 30, and 45 deg, and a constant viewing angle of 0 deg, were obtained. These are shown in Figs. 3–5. Note that as the rotational rate increases (from a to e in a series), flow evolves from natural to mixed, to forced convection.

The typical fringe patterns which represent natural convection (Re = 0) are shown in Figs. 3a, 4a, and 5a. When the heated sphere is not rotated, as in the above cases, free thermal boundary flow occurs in the form of a steady plume associated with fluid rising from the lower parts of the sphere. The width of the plume decreases with increasing vertical distance from the sphere surface and gradually dissipates due to viscous effects and a reduction in the buoyancy force. The temperature field extends over a narrow zone in the immediate vicinity of the sphere surface, forming a thermal boundary layer. Such natural convection flow and heat transfer characteristics were discussed by Farouk,[11] who also theoretically predicted isothermal contours similar to those shown in Figs. 3a, 4a, and 5a. His calculations were based on the Navier-Stokes and Boussinesq equations (see Figs. 6a and 6b).

The various fringe patterns representing mixed convective flow are shown in Figs. 3b–d, 4b–d, and 5b–d. Note that the sphere is rotated slowly, a weak centrifugal force is induced on the thermal plume, causing it to widen slightly. As one goes to higher rotational speeds, the buoyancy parameter[10,11] Gr/Re^2 decreases, and the buoyancy effect becomes more and more comparable to the centrifugal effect, bringing about remarkable changes that complicate the convection flow and result in a distorted upward plume. This distortion was also predicted by Farouk,[11] in his numerical analysis of such systems (see Figs. 6c and 6d).

It is noted that after flow separation, a very complicated, irregular and unsteady turbulent zone, which to our knowledge has not been reported before, was observed (see Figs. 3d–5d). In those situations where $\alpha < 90$ deg, the turbulent zones were observed on the upper half of the sphere. Unfortunately, due to equipment limitations, it was extremely difficult to run experiment at α = 90 deg. The location of turbulent zones in these cases, were observed either in the left or right half of the sphere, depending on the positive or negative deviation of α from 90 deg.

Another interesting phenomenon is the appearance of an eruption jet near the sphere's equatorial plane, as predicted by Farouk[11] (see Figs. 3e–5e). It arises from the impingement of two flows upon each other,[1] which severely hampers heat dissipation. A relatively massive eruption jet (300 km wide) occurs near the earth's equator,[19] and is known as the Cromwell current. Note the similarities between the predicted isotherms and streamlines in Fig. 6e with those of the holographic visualization in Fig. 6f.

B. Thermal Boundary Layer

A distinct thermal boundary layer surrounding most of the sphere's surface is a common feature in all the interferograms,

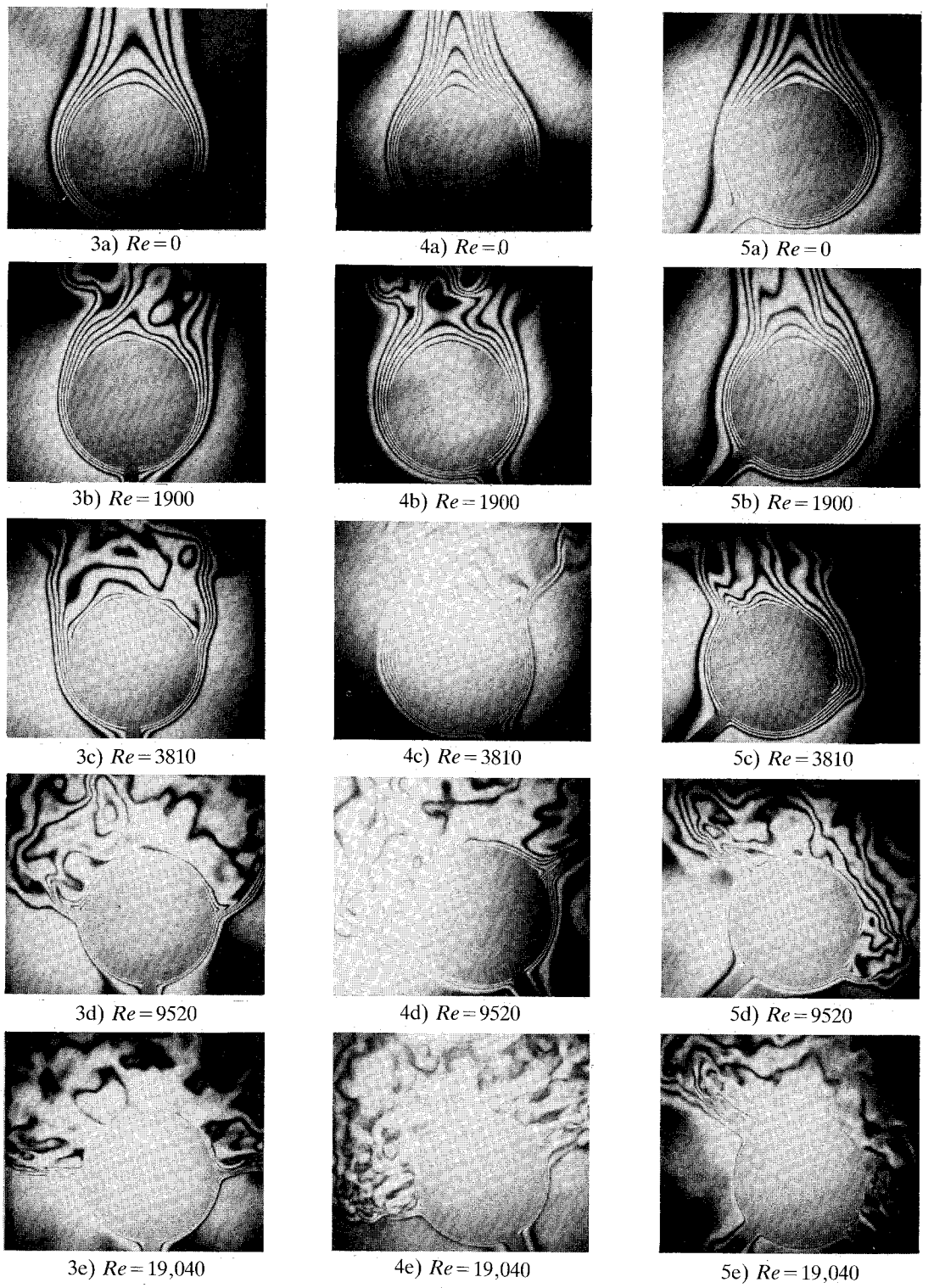

Figs. 3–5 Holographic visualization pictures of convective thermal flowfields around a heated rotating sphere at different values of *Re* and α: 3a–e for α = 0 deg; 4a–e for α = 30 deg; 5a–e for α = 45 deg.

even those in which a turbulent zone appears. The thickness of this layer was found to vary with *Re* and α, as shown in Fig. 7 for α = 0 deg and α = 45 deg. Here, the thickness can be seen to decrease as *Re* increases; the current is driven by rotation of the sphere to approach the sphere surface. The thickness of the thermal boundary layer was determined by measuring the distance from the sphere surface to the outermost detectable fringe, rather than by complicated holographic tomography.[17,20] This simple method was found to be in good agreement (2.5% deviation) with those values calculated from the formal definition of the thermal boundary layer which is defined as the thickness for which the ratio $[(T_s - T)/(T_s - T_\infty)] = 0.99$, ($\alpha$ = 0 deg). Here T_s is the sphere surface temperature, T_∞ the ambient temperature, and T the temperature at the leading edge of the boundary layer (reconstructed by Abel inversion[17,21]). A three-dimensional quantitative investigation of this subject by tomographic reconstruction will be conducted in the near future.

The distribution of the thermal boundary-layer thickness vs the angular distance θ along a meridian was also examined by detailed three-dimensional holographic observations, and the results are given in Fig. 8. Note that the thickness gradually increases from a minimum value at the south pole (0 deg) to a maximum value at the equator (90 deg), just like

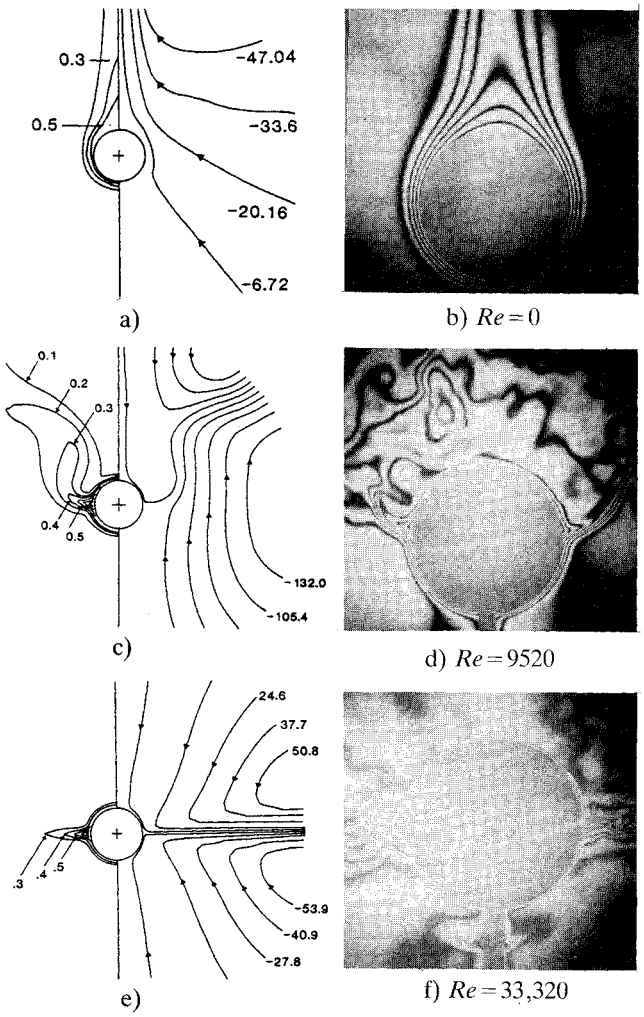

Fig. 6 a) Natural convection (for $Re = 0$, $Gr = 1.38 \times 10^4$) by theoretical prediction [after Farouk (1985)[11]]. (left: isotherms, right: streamlines); b) natural convection (for $Re = 0$, $Gr = 3.21 \times 10^5$) by holographic visualization; c) mixed convection (for $Re = 1173$, $Gr = 1.39 \times 10^4$) by theoretical prediction [after Farouk (1985)[11]], (left: isotherms, right: streamlines); d) mixed convection (for $Re = 9520$, $Gr = 3.21 \times 10^5$) by holographic visualization; e) Eruption jet near the equator plane by theoretical prediction ($Re = 1173$, $Gr = 0$) [after Farouk (1985)[11]], (left: isotherms, right: streamlines); f) Eruption jet near the equator plane by holographic visualization ($Re = 33{,}320$, $Gr = 3.21 \times 10^5$).

the velocity boundary layer distribution reported by Kreith[10] and Howarth[2] (Fig. 8c). For all cases in which $\alpha \neq 0$ deg, the thermal boundary layer appears to be asymmetrically distributed about the rotational axis, as shown in Fig. 8b. This effect disappears when the rotational rate is high enough ($Re > 9000$, $Gr = 3.07 \times 10^5$) to uniformly distribute the thickness of the thermal boundary layer along a meridian, even though the rotational angle is large. It is only near the equator where the flow current separates to form an eruption jet and the thickness broadens out.

C. Separation and Reattachment

As the rotating speed of the sphere is increased, the thermal boundary layer detaches from the sphere surface until it flows separately. This phenomenon is best seen in Fig. 9 (angular distance $\theta = 94$ deg). A similar phenomenon was reported by Hauf and Grigull[22] on the convection flow around a heated rotating horizontal cylinder. After separation, reattachment of the thermal boundary layer can occur ($\theta = 134$ deg (Fig. 9)), as was observed when $Re = 3500 \sim 6000$ and $\alpha = 45$ deg.

According to Fig. 10, the movement of fluid in the thermal boundary layer can simply be a result of force F_r, calculated

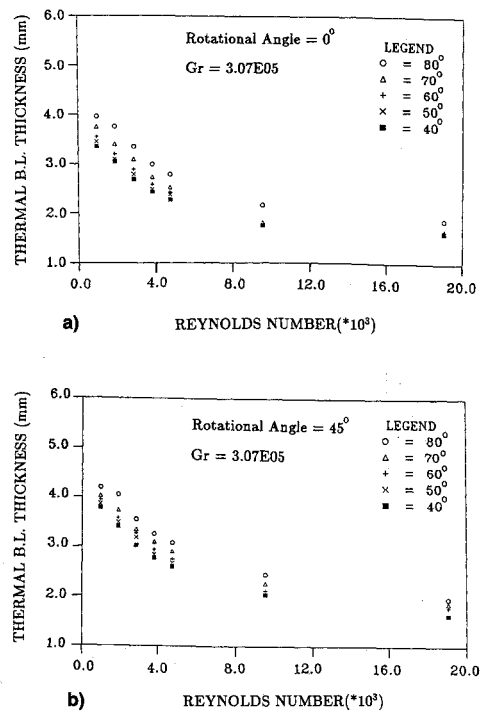

Fig. 7 Thermal boundary-layer thickness vs Reynolds number: a) $\alpha = 0$ deg; b) $\alpha = 45$ deg.

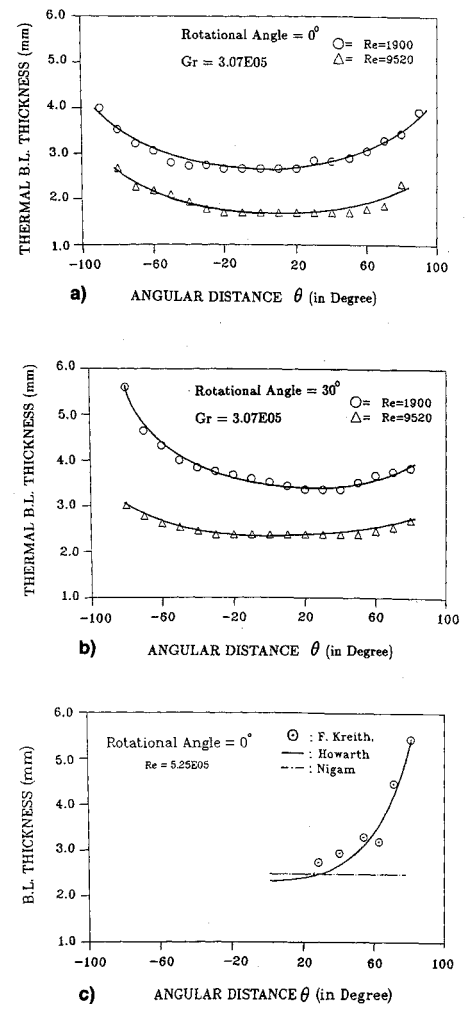

Fig. 8 Thermal boundary layer-thickness vs angular distance θ: a) $\alpha = 0$ deg; b) $\alpha = 30$ deg; c) velocity boundary-layer thickness vs angular distance θ for $\alpha = 0$ deg by Kreith et al.[10]

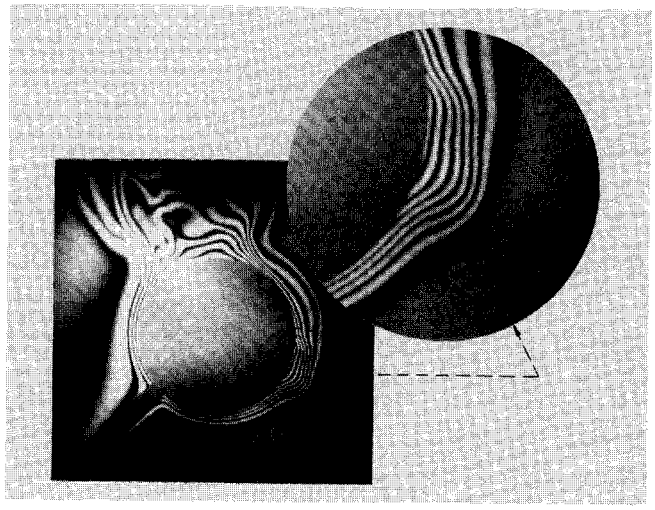

Fig. 9 Holographic visualization picture for separation and reattachment (Re = 4760; Gr = 3.21 × 10^5; α = 45 deg).

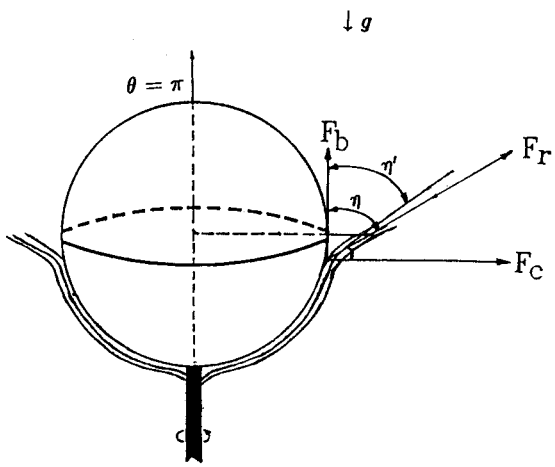

Fig. 10 Schematic diagram of centrifugal force and buoyancy force acting to the fluid.

Table 1 Comparison between calculated angle η and measured separation angle η' (refer to Fig. 10)

Rotation Reynolds number	Calculated angle η, deg	Measured angle η', deg
3,810	22.0	24
4,760	32.3	38
9,520	68.2	65
19,040	84.3	82

from the centrifugal force (F_c) and buoyancy force (F_b). F_c increases with rotational speed. When the centrifugal force is large enough to overcome the local shear stress at the wall, separation occurs. This brief explanation for separation was found from a comparison between angles η and η' (see Fig. 10). The direction of F_r is represented by η, while η' is the tangential angle of the thermal boundary layer measured at its point of separation from the fringe pattern. The results are presented in Table 1 in which η was calculated by the formula (α = 0 deg):

$$\eta = \tan^{-1} \frac{\text{centrifugal acceleration}}{\text{buoyancy acceleration}}$$

In most cases the calculated results agree with the measured data. Deviations can be attributed to the limitations of the rotational speed measuring equipment and the approximate formula $g(T - T_\infty)/T_\infty$ used in calculating buoyancy acceleration.

As the Reynolds number increases, the separation points at both sides of the sphere will shift. For the case of α = 0 deg, the separation points at both sides of the sphere shift symmetrically towards the equator as the rotational speed increases. With inclined rotation, the two separation points exhibit different shifting behaviors. The separation point on the upper half of the sphere hardly changes position as Reynolds numbers increase. While the other separation point, located on the lower half of the sphere away from the equator, shifts quickly towards the equator. For inclined rotation, the shifting behavior can be explained with reference to F_c and F_b. In the upper half of the sphere, both the centrifugal and buoyancy forces are angled upwards, meaning that F_r also acts in an upward direction and thus it does not substantially affect the location of the separation point. In the lower half of the sphere, however, F_c is somewhat opposite to F_b. Thus, as the centrifugal force increases, the direction of F_r shifts from upwards to downwards, causing the lower separation point to approach the equator. This shifting behavior is clearly illustrated in Fig. 11.

A three-dimensional holograph was employed to measure the spatial distribution of separation points from different viewing angles for the case of α = 30 deg, Re = 4760, and Gr = 3.21 × 10^5. The measured data are plotted as a linear relationship shown in Fig. 12. The spatial distribution of separation points around the sphere surface can be said to form a ring around the sphere whose angles of inclination changes for different rotational angles and Reynolds numbers.

The critical Reynolds numbers for separation are presented in Table 2, which shows that these critical values decrease as α increases. It has been also noted that these critical values are strongly dependent on the values of Grashof number and the diameter of the sphere.

The reattachment phenomenon was observed most often in the test range of Re = 3500 ~ 6000. This phenomenon occurs due to the fact that as a separated fluid moves away from the sphere wall, the centrifugal force acting on it becomes weaker while the F_b becomes stronger, causing the separated fluid to approach the sphere surface once more (see Fig. 9). Owing to this fluid reattachment, it is probable that heat is difficult to dissipate at the reattachment point.

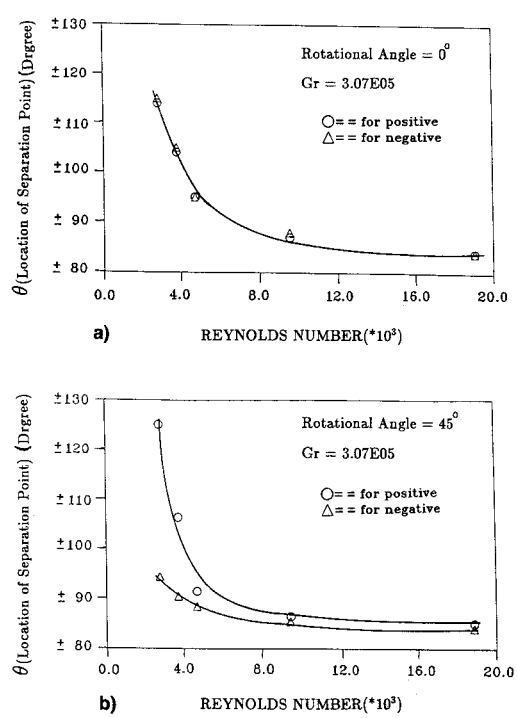

Fig. 11 Relationships between locations of separation point and the rotational Reynolds number: a) α = 0 deg; b) α = 45 deg.

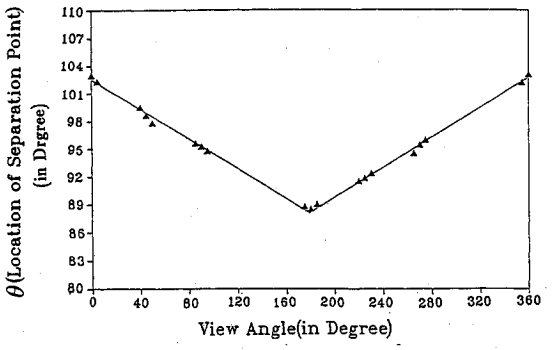

Fig. 12 Spatial distribution of separation points Re = 4760, α = 30 deg; Gr = 3.21E05.

Table 2 Critical rotational Reynolds numbers for separation

Rotation angle, deg	Grashof number	Critical rotational Reynolds number for separation
0	3.21×10^5	4500
30	3.21×10^5	4000
45	3.21×10^5	3000

D. Turbulent Zone

Besides eruption jets, like the one described above, turbulent zones can also be observed downstream of separation points. A physical explanation of this phenomenon, based on qualitative analysis of interactions between centrifugal and buoyancy forces, is given below.

For an unheated rotating sphere, Stokes[1] predicted that a flow current would be induced around a sphere purely by centrifugal effect (see Fig. 6e). However, when a heated sphere is rotated, in addition to the presence of Stoke's flow current (centrifugal current), another flow current arises from the buoyancy effect. The two flow currents move in the same direction in the lower half of the sphere, but in opposite directions in the upper half. For small rotational speeds, the downward flow current (centrifugal current) acting on the upper half of the sphere is weaker than the buoyancy current which forms an upward thermal plume. As the rotational speed is increased, the downward current induced by the centrifugal effect becomes stronger. When its strength is comparable to that of the buoyancy current, the two opposite flow currents in the upper half of the sphere come into collision, generating a very complicated, irregular turbulent flow which includes unsteady vortices after separation. It is also evident from holographic observation that the area covered by the turbulent zone grows as Re increases. It is reasonable that in a turbulent zone the heat transfer rate can increase considerably and could have a influence on the averaged Nusselt number.

If Re increases continuously, the buoyancy effect will be relatively weaker than the centrifugal effect. If the centrifugal effect becomes strong enough, the turbulent zone disappears (see Fig. 6f, Re = 33,320).

IV. Conclusion

Three-dimensional diffuse-illumination holographic interferometry was successfully employed to visualize the mixed convective flow around a heated rotating sphere.

The holographic interferograms clearly capture such interesting flow phenomena as flow separation, reattachment, turbulent zones, and eruption jets. Especially noteworthy is the observed turbulent zone appearing in the upper half of the sphere which, to our knowledge, was never reported or predicted before.

Physical explanations corresponding to these flow phenomena are discussed, based on the interactions between the buoyancy and centrifugal forces generated by a heated rotating sphere.

Quantitative results of thermal boundary-layer thickness distribution, locations of separation points, and critical rotational Reynolds numbers for separation, are presented and compared with previous theoretical predictions.

Acknowledgment

The authors gratefully acknowledge the financial support of the National Science Council of the Republic of China under Contract NSC80-0401-E-006-47.

References

[1]Kreith, F., "Convection Heat Transfer in Rotating System," *Advances in Heat Transfer,* Vol. 5, 1968, pp. 129–251.

[2]Howarth, L., "Note on the Boundary Layer on a Rotating Sphere," *Philosophical Magazine,* Ser. 7, Vol. 42, 1951, pp. 1308–1315.

[3]Nigam, S. D., "Note on the Boundary Layer on a Rotating Sphere," *Zeitschrift fuer Angewandte Mathematik und Physik,* Vol. 5, 1954, pp. 151–154.

[4]Kobashi, Y., "Measurements of Boundary Layer of a Rotating Sphere," *Journal of Science,* Hiroshima Univ., A20, 1957, pp. 149–156.

[5]Sullivan, J. A., "Laminar Flow Around a Rotating Sphere in an Infinite Environment," Ph.D. Thesis, Univ. of Colorado, Boulder, CO, 1960.

[6]Kohama, Y., and Kobayashi, R., "Boundary Layer Transition and the Behavior of Spiral Vortices on Rotating Sphere," *Journal of Fluid Mechanics,* Vol. 137, 1983, pp. 153–164.

[7]Dennis, S. C. R., Singh, S. N., and Ingham, D. B., "The Steady Flow Due to a Rotating Sphere at Low and Moderate Reynolds Numbers," *Journal of Fluid Mechanics,* Vol. 101, 1980, pp. 257–280.

[8]Singh, S. N., "Heat Transfer by Laminar Flow from a Rotating Sphere," *Applied Scientific Research,* Vol. 13, 1960, pp. 197–205.

[9]Nordlie, R., and Kreith, F., "Convection Heat Transfer from a Rotating Sphere," *International Development in Heat Transfer,* American Society of Mechanical Engineers, New York, 1961, pp. 461–467.

[10]Kreith, F., Roberts, L. G., Sullivan, J. A., and Sinha, S. N., "Convection Heat Transfer and Flow Phenomena of Rotating Sphere," *International Journal of Heat and Mass Transfer,* Vol. 6, 1963, pp. 881–895.

[11]Farouk, B., "Mixed Convective Flows Around a Slowly Rotating Isothermal Sphere," *Transactions of the American Society of Mechanical Engineers: Journal of Heat Transfer,* Vol. 107, 1985, pp. 431–438.

[12]Rajasekaran, R., and Palekar, M. G., "Mixed Convection About a Rotating Sphere," *International Journal of Heat and Mass Transfer,* Vol. 28, 1985, pp. 959–968.

[13]Hatzikonstantinou, P., "Unsteady Mixed Convection About Aporous Rotating Sphere," *International Journal of Heat and Mass Transfer,* Vol. 33, 1990, pp. 19–27.

[14]Lien, F. S., Chen, C. K., and Cleaver, J. W., "Mixed and Free Convection over a Rotating Sphere with Blowing and Suction," *Transactions of the American Society of Mechanical Engineers: Journal of Heat Transfer,* Vol. 108, 1986, pp. 398–404.

[15]Palec, G. L., and Daguenet, M., "Laminar Three-Dimensional Mixed Convection About a Rotating Sphere in Stream," *International Journal of Heat and Mass Transfer,* Vol. 30, 1987, pp. 1511–1523.

[16]Chen, T. S., and Mucoglu, A., "Analysis of Mixed Forced and Free Convection About a Sphere," *International Journal of Heat and Mass Transfer,* Vol. 20, 1977, pp. 867–875.

[17]Vest, C. M., *Holographic Interferometry,* Wiley, New York, 1979.

[18]Hariharan, P., *Optical Holography,* Cambridge University Press, London, 1984.

[19]Long, R. R., "A Turbulent Equatorial Jet," *Journal of Fluid Mechanics,* Vol. 11, 1961, pp. 465–477.

[20]Tieng, S. M., and Chen, H. T., "Holographic Tomography by SART and its Application to Reconstruction of 3-D Temperature Distribution," *Wärme-und Stoffübertragung,* Vol. 26, 1990, pp. 49–56.

[21]Tieng, S. M., and Lai, W. Z., "Temperature Measurement of Reacting Flowfield by Phase Shift Holographic Interferometry," accepted by *Journal of Thermophysics and Heat Transfer,* Vol. 6, No. 2, 1992.

[22]Hauf, W., and Grigull, U., "Optical Methods in Heat Transfer," *Advances in Heat Transfer,* Vol. 6, 1970, pp. 133–366.